https://doi.org/10.48048/tis.2024.8110

The Impact of Activation Heating Rate on Pore Structure in Teak Sawdust-Derived Activated Carbon and Its Application in Methylene Blue Adsorption

I Gusti Agung Kade Suriadi[1,2], Dewa Ngakan Ketut Putra Negara[3,*], Tjokorda Gede Tirta Nindhia[3], I Ketut Adi Atmika[3], I Made Dwi Budiana Penindra[2] and I Made Gatot Karohika[3]

[1]Doctoral Study Program of Engineering Science, Faculty of Engineering, Udayana University, Denpasar, Bali 80234, Indonesia
[2]Industrial Engineering Department, Udayana University, Bukit Jimbaran, Bali 80361, Indonesia
[3]Mechanical Engineering Department, Udayana University, Bukit Jimbaran, Bali 80361, Indonesia

([*]Corresponding author's e-mail: devputranegara@unud.ac.id)

Received: 23 February 2024, Revised: 14 March 2024, Accepted: 21 March 2024, Published: 20 August 2024

Abstract

Activated carbon (AC) is a multifunctional adsorbent with a high adsorption capacity because of its pore structure comprising a large pore volume and surface area. However, its pore structure properties are largely influenced by the chemical composition and manufacturing conditions of the raw material. This study examined the effect of activation heating rate parameter on pore structure and methylene blue adsorption in teak sawdust AC. The adsorbent was dehydrated, carbonized and activated at 105, 750 and 700 °C for 2 h, 50 min, and 6 to 14 °C/min, with a nitrogen flow rate of 200 mL/min for 50 min. Several characterizations were carried out to identify pore structure, proximate substance, functional groups, surface morphology, and methylene blue-adsorption capacity of AC. The results showed that activation heating rate with the best properties and capacity of MB adsorption were adsorbed at a peak of 10 °C/min. AC obtained has a C-C aromatic rings functional group, an amorphous crystal structure, an interplanar length of 3.03 Å, 75.74 % fixed carbon, pore surface area of 126.279 m^2/g, pore volume of 0.235 cc/g, and a multimodal micropore-mesopore size distribution. This is in addition to adsorption capability of 13.48 mg/g for methylene blue.

Keywords: Activation heating rate, Activated carbon, Adsorption, Teak sawdust waste, Methylene blue

Abbreviations

AC = Activated carbon
AC-H6 = activated carbon activated with activation rate of 6 °C/min
AC-H8 = activated carbon activated with activation rate of 8 °C/min
AC-H10 = activated carbon activated with activation rate of 10 °C/min
AC-H12 = activated carbon activated with activation rate of 12 °C/min
AC-H14 = activated carbon activated with activation rate of 14 °C/min
S_{BET} = specific surface area

V_P = specific pore volume
D_P = average pore diameter
PSD = pore size distribution
MB = methylene blue
FTIR = Fourier transform infrared
XRD = X-Ray Diffraction
SEM = Scanning Electron Microscope

Introduction

Activated carbon (AC) is a highly porous material, characterized by large adsorption capacity, capable of attracting and retaining organic molecules [1]. AC has a complex pore structure, specific surface area, great chemical stability, and numerous oxygen-containing functional groups on the surface [2]. These properties enabled adsorption of a wide range of compounds, making AC indispensable across various applications, including adsorption of motorcycle emissions [3], CO_2 capture [4-7], removal of methylene blue [8-10], battery electrodes [11], methane storage [12], supercapacitor [13-15], removing water impurities [16], adsorption of drugs [17-19], etc. However, due to the diverse range of applications, AC is in high demand and holds promising growth prospects.

The characterization of AC using structural formulation or chemical analysis, poses certain difficulties due to the complex and structurally imperfect nature. This was as a result of the irregular, and randomly oriented structure, lacking directional relationships in single graphite crystals [20]. Furthermore, understanding the properties of raw materials and manufacturing methods is critical for producing AC with superior attributes designed for certain applications.Achieving this objective requires conducting experiments and characterizing AC to determine appropriate usage. Understanding features such as pore size is crucial because it significantly influences adsorption ability. While AC can effectively capture organic chemical substances that are smaller or similar in size to pore, larger molecules may not be easily adsorbed [1].

AC has a high adsorption capacity for organic pollutants; however, the commercial use increases the overall cost of the process. This is mainly because AC is often derived from non-renewable resources such as coal, lignite, polymers, and petroleum wastes, which are becoming increasingly scarce. To address this challenge, there is a growing interest in synthesizing AC from biomass waste sources that are readily available. Biomass is an attractive option because it is readily available, inexpensive, and contains a high concentration of lignin and cellulose. Several biomass sources, including bamboo [21,22], coconut [23,24], rice husk [25], coffee ground [10,26,27], and shallot peel [28], have been converted into AC. In addition, teak sawdust is a rarely used biomass waste with high fix carbon content [29]. Teak sawdust also has the potential to be used as raw material for AC production, allowing waste to be converted into usable products

To synthesize AC, there is need to understand the ideal parameters for the production process. Furthermore, the chemical composition of the raw material, and selected manufacturing parameters, significantly affect the AC quality. This AC is typically produced using dehydration, carbonization, and activation processes. Dehydration is a process of reducing the water content in raw materials, while carbonization converts it into charcoal with a high-fix carbon content and less volatile, initiating pore formation through thermal decomposition. The final activation step, broadens existing pore, thereby creating new ones, and removing pore-clogging impurities, resulting in a well-defined pore structure and a large surface area. The parameters including temperature, time, type of activating agent, and method are critical determinants of AC quality. While the effect of carbonization heating rate on the properties and

adsorption capacity of AC had been extensively investigated [29-33], studies on the impact of activation heating rate are relatively scarce. This parameter is essential, because a rapid rate reduces pore expansion, formation of new holes, and wasteful gasses transported through the charcoal. A sluggish activation rate results in a waste of time, energy, and activating chemicals, as well as a higher probability of pore collapse. Therefore, determining the optimal activation heating rate is essential in the production of AC

The aim of this study is to investigate the impact and optimal activation heating rate on pore structure and methyl blue adsorption of AC, produced from sawdust. The observed pore structure comprised specific surface area (S_{BET}), specific volume (V_P), size distribution (PSD), and average diameter (D_P). In addition, the study investigated various other characteristics of AC, such as functional groups, interplanar lengths, and proximate compositions. The novelty of the study is to determine the optimal activation heating rate for converting teak sawdust waste into high-quality AC.

Materials and methods

Materials and ACs preparation

The precursor used is teak sawdust waste collected from furniture craftsmen in the Kelungkung-Bali region, Indonesia. Previous studies stated that the precursor constituted 8.37 % moisture, 71.23 % volatile matter, 1.84. % ash, and 18.56 % fixed carbon [29]. In addition, the proximate composition of teak sawdust is in line with the study conducted by Gupta [34]. The production process stated with drying a total of 400 g of teak sawdust powder in an electric furnace at 105 °C for 2 h. The sample obtained was cooled to room temperature, before it was carbonized. The carbonization process required filling the reactor with dehydrated teak sawdust powder, and then heated to 750 °C for 50 min in an electric furnace. Furthermore, the resulting charcoal is then sieved through a mesh size of 60.50 g of meshed charcoal were placed in the reactor and subjected to activation by being kept in an electric furnace. The electric furnace was heated to 700 °C at a rate of 6 °C/min, then fed with nitrogen at rate of 200 mL/min using a flow mass controller and held for 50 min. Subsequently, the sample was cooled in the furnace until it reached room temperature, and the resulting AC collected in an air-tight plastic bottle. The same procedure was repeated for activation rates of 8, 10, 12, and 14 °C/min, producing AC samples denoted by the symbols AC-H6, AC-H8, AC-H10, AC-H12, and AC-H14, respectively.

Activated carbon characterization

A variety of tests were conducted to analyze the properties of AC. The proximate composition of AC was determined using a TGA 701 device equipped with ASTM D7582 MVA Biomass. The functional groups and surface morphology were identified using FTIR IRPrestige-21 and SEM-JSM-651OLA instruments, respectively. The interplanar distance of AC was measured using an XRD PANalytical-X'Pert PRO equipment with a diffraction angle range of 10 to 90 °. Pore structure of AC, including S_{BET}, V_P, and D_P, were evaluated using adsorption isotherm test conducted by applying a Quantachrome Nova Instruments 1200e equipment. S_{BET} was determined using the Brunaeur-Emmet-Teller (BET) method at a relative pressure between 0 and 0.32. Total pore volume was obtained for pore with a radius less than 186.5 nm at a relative pressure of 0.994.

Methylene blue tests

Ultraviolet-visible (UV-Vis) spectroscopy was used to investigate adsorption of methyl blue. A 5-ppm MB solution was produced, and 0.1 g of AC was mixed with 20 mL of the solution. After 20 min of mixing with a magnetic stirrer, the mixture was left for 2 h until equilibrium was attained. Subsequently,

the solution was filtered with filter paper, and the wavelength of filtrate measured at 664 nm. Adsorption quantity was determined using Eq. (1) [35], where q_t (mg/g) is adsorption capacity (mg/g), c_o (mg/L) is the initial concentration of the solution, c_t (mg/L) is the concentration at time t, V (L) is the volume of the solution, and m (g) is the mass of AC. The test was repeated 3 times for each activation heating rate.

$$q_{t=\frac{(C_0-C_t}{m})V} \quad (1)$$

Results and discussion

TGA analysis

The results of TGA test in **Table 1**, show the impact of carbonization on the material composition. This process led to an increase in carbon fix content and a decrease in volatiles compared to the precursor. The change was attributed to the thermal decomposition, occurring during heating, which reduced the volatile content while increasing carbon fix. The composition is in line with the results reported by Gupta, who examined the pyrolysis of teak sawdust at various temperatures, producing char with moisture, volatile matter, ash, and fixed carbon contents ranging from 1.73 to 2.67, 9.37 to 25.61, 7.50 to 12.22 and 64.22 to 76.68 %, respectively [34]. Meanwhile, the TGA composition showed all samples met the Indonesian National Standard (SNI 06-3730-1995), that powdered AC must have a maximum of 25 % volatile matter, 15 % moisture, 10 % ash, and 65 % fixed carbon content. Moisture and ash composition are affected by activation heating rate in a fluctuated manner, while volatile matter and fixed carbon follow a parabolic pattern. However, moisture content decreases from 6 to 10 °C/min, then increases at 12 °C/min before declining again at 14 °C/min. Activation at lower rate relatively 6 to 8 ºC/min resulted in increased ash content, which reduced with a higher heating rate of 10 °C/min. In addition, increasing heating rate from 10 to 12 and 14 °C/min raised the ash content. Volatiles followed an upward parabolic pattern, and fixed carbon content adhered to a downward parabola. The minimum and maximum volatile (6.96 %) and fixed carbon values (75.74 %) were achieved at activation rate of 10 °C/min. Based on TGA composition, AC-H10 had the best, with the highest fixed carbon 75.74 %, lowest moisture content 8.3 %, ash 6.96 %, and volatile matter 9 %.

Table 1 The proximate composition of ACs.

Sampel	Moisture (%)	Volatile (%)	Ash (%)	Fix carbon (%)
Char	8.8	11.58	9.92	69.7
AC-H6	10.78	13.2	5.97	70.05
AC-H8	8.8	10.58	9.92	70.70
AC-H10	8.3	9	6.96	75.74
AC-H12	9.07	9.71	9.63	71.59
AC-H14	9.02	9.97	10.19	70.82

FTIR and XRD analysis

Figure 1 shows the FTIR analysis of charcoal and AC. The spectrum of AC differs significant from charcoal, due to the dehydration and breakdown of complex lignocellulosic groups into simpler ones.

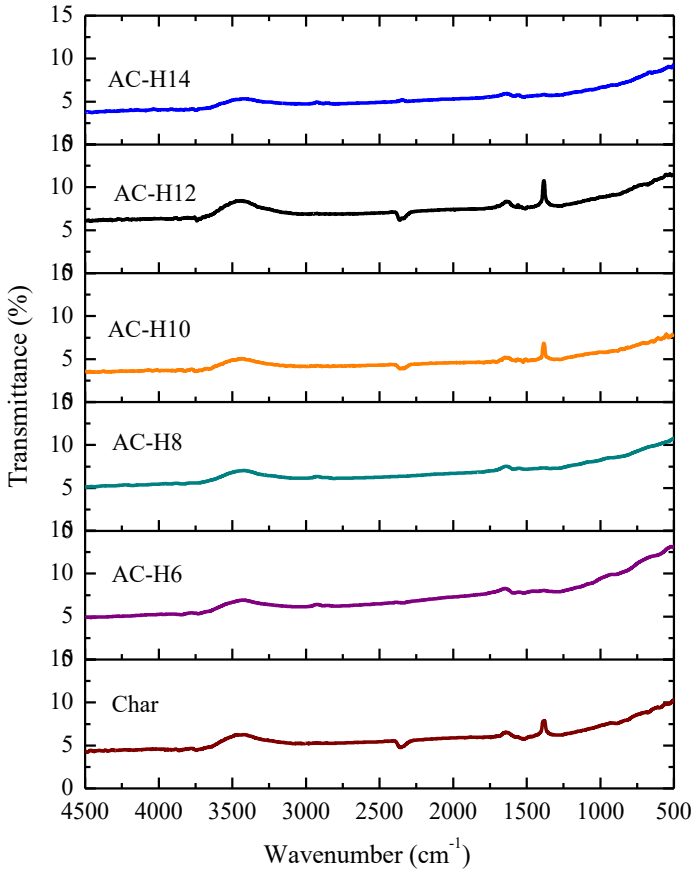

Figure 1 FTIR spectra of charcoals and ACs.

An overview of the wavenumber peaks and functional groups of the samples are shown in **Table 2**. However, determining the influence of activation heating rate on AC functional groups is challenging due to the random relationship with heating rate. A significant observation was the consistent presence of aromatic ring C−C functional group across all AC within the wave number range of 1516.11 to 1591.34 cm^{-1}. The functional group, characterized by a hexagonal shape, was formed during the carbonization-activation process. Aromatic rings, or compounds, are hydrocarbons with benzene or similar ring configurations. The six carbons in benzene are joined in a ring, resulting in a planar geometry of a regular hexagon where all C−C bond distances are equal.

Table 2 FTIR peaks and functional groups of charcoal and ACs.

Sampel	**FTIR peaks (cm^{-1})**				
Char			2358.08	1526.72	599.89
AC-H6	3730.49			1591.34	477.40
AC-H8	3834.63	2883.7		1588.45	461.90
AC-H10			2353.26	1527.49	530.43
AC-H12	3745.92		2354.22	1587.49	
AC-H14		2882.74		1516.11	
Functional group	O−H Hydroxyl	C−H Aldehyde	C−H Aliphatic stretching	C−C Aromatic ring	C−H Aromatic hydrocarbon

Figure 2 shows the correlation between angle 2θ and diffraction intensity at angular distances ranging from 10 to 90 °. In addition, the position of peak intensity and interplanar distance are shown in **Table 3**. The diffraction strength increases as the number of crystal planes rises, with each plane represented as a peak in the XRD pattern. This arises from the scattering of x-rays by individual atoms. Constructive interference occurs when 2 or more waves have the same phase, consequently x-ray scattering reinforces each other, resulting in diffraction peaks. The higher the strength of the x-ray diffraction, the more the uniformly scattered x-rays by crystalline structure. Both charcoal and AC have broad and weak diffraction peaks at angles (2θ) within the range of 10 to 30 °, showing an amorphous carbon structure [13]. This observation is in line with the results of Im [36], who reported a similar XRD pattern for coke-AC. The influence of activation rate produced the same diffraction pattern because all samples were amorphous carbon materials with slightly variable diffraction intensity, peak positions, and interplaner distances, as shown in **Table 3**. The diffraction peak typically varies from 36.54 to 65.87 (cts), at angles (2θ) ranging from 29.27 to 29.39 °, with interplanar lengths (d-spacing) between 3.03 and 3.04 Å. The highest and lowest peaks were observed in char, and AC-H10, respectively. This discrepancy showed that AC-H10 was the most amorphous compared to other samples.

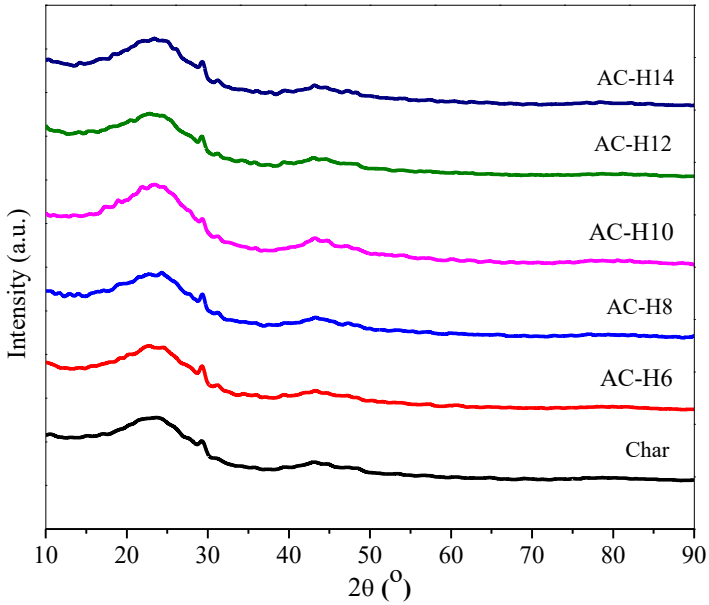

Figure 2 XRD graph of chars and ACs.

Table 3 Peak intensity, position, and interplanar distance on the 2θ scale derived from XRD test.

Sampel	Position (°)	Height (cts)	d-spacing (Å)
Char	29.36	65.87	3.03
AC-H6	29.39	60.04	3.03
AC-H8	29.34	47.36	3.04
AC-H10	29.36	36.54	3.03
AC-H12	29.27	41.64	3.04
AC-H14	29.35	40.95	3.04

SEM analysis

Figure 3 shows that the surface morphology of the AC have increased number of pores, compared to charcoal although the changes were difficult to detect in samples AC-H6 and AC-H12. Transverse pore was plainly visible on AC-H8 and AC-H10 represented with white elliptical lines, while longitudinal pore was spotted on Char and AC-H12. The pore was identified in both the transverse and longitudinal orientations on AC-H14, but only in small numbers on AC-H6. AC-H10 sample had the greatest change in pore structure, with prominently visible ones occurring in large number compared to the others. The heating rate of 10 ºC/min effectively enlarged existing pore, cleaned tar residues, and produced new ones, thereby resulting in the best surface morphology when compared to other samples. The SEM image lacked quantitative information regarding the number of pore, volume, or diameter of AC, although it can be used to support the desired qualities. Adsorption isotherm test in **Table 4** provided quantitative information on the number of pore, volume, and pore diameter of AC, which was used to determine the connection between heating rate, pore structure, and adsorption performance.

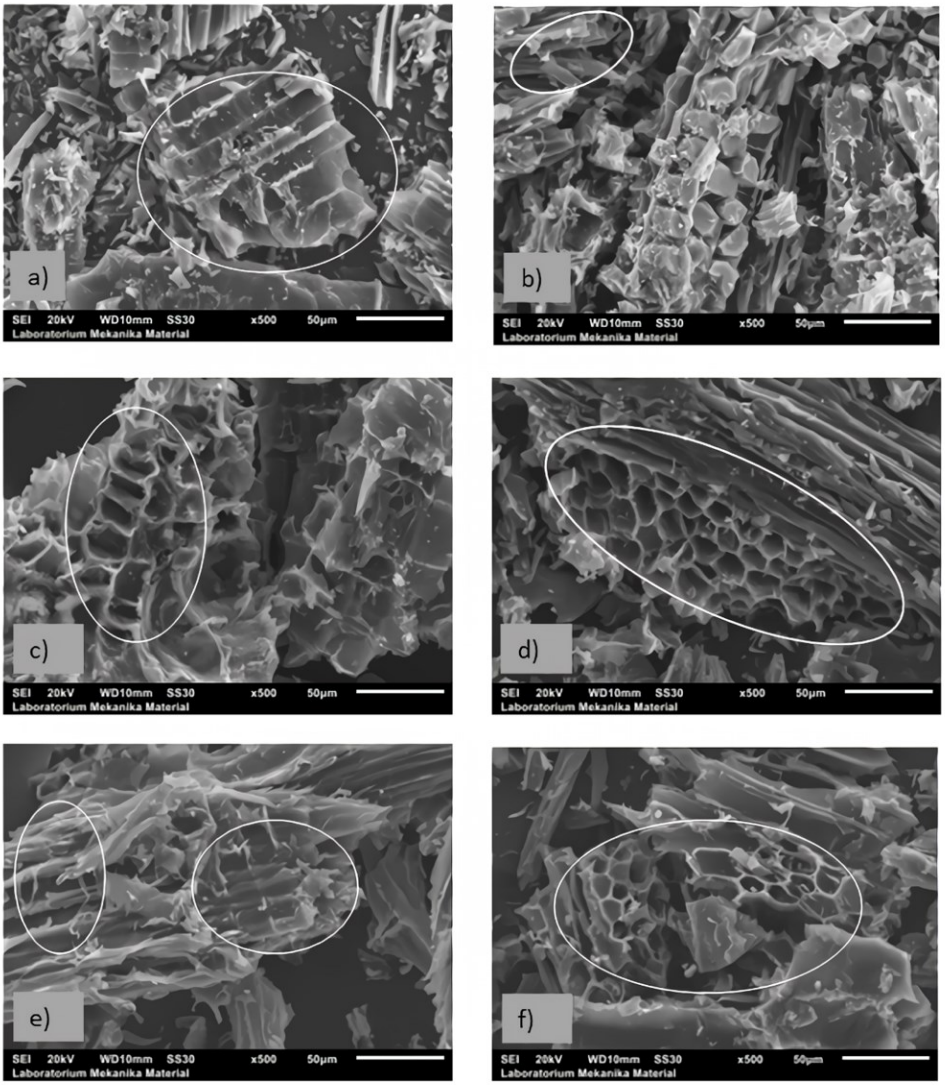

Figure 3 SEM images of samples: (a) Char, (b) AC-H6, (c) AC-H8, (d) AC-H10, (e) AC-H12, and (f) AC-H14.

Adsorption isotherm of AC

Figure 4 shows adsorption isotherm curves for both charcoal and AC, depicting the relationship between nitrogen adsorption capacity and various relative pressures. Both materials showed similar adsorption patterns, with higher relative pressures, leading to increased nitrogen adsorption. The differences are in the amount of nitrogen adsorbed by each active carbon at varying relative pressures. According to the pattern, the majority of AC samples had mesopore-sized holes due to a lack of significant adsorption at a relative pressure of less than 0.1. The fulfillment process does not occur in the micropore region, therefore there are relatively few active carbon micropore. Char had the lowest adsorption rate across all relative pressure ranges because the pore was coated in carbonization products, particularly tar, which led to lack of porosity, including pore surface area and volume [37]. The interpretation was supported by the quantitative test results shown in **Table 4**.

The activation heating rate consistently produced the same adsorption isotherm curve pattern. However, at a relative pressure of 1, it generated a parabolic nitrogen adsorption pattern. The nitrogen adsorption capacity increased from AC-H6 to AC-H10, before declining from AC-H10 to AC-H14. The peak adsorption occurred in AC-H10 AC, which was approximately 161.25 cc/g. The best activation heating rate was 10 °C/min, which produced maximum nitrogen adsorption. The observation was supported by additional properties, including appropriate TGA composition and AC-H10 morphology.

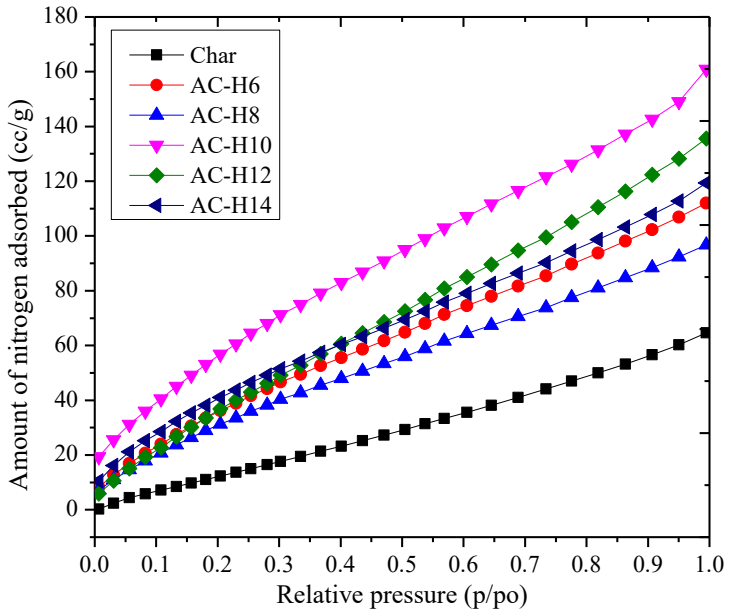

Figure 4 Adsorption isotherm of char and ACs.

PSD of AC

Figure 5 shows pore size distribution curves for both charcoal and AC. These curves depicted the relationship between the amount of nitrogen absorbed at the various pore sizes. Char, AC-H8, and AC-H12 showed monomodal distributions characterized by a single adsorption peak located in the mesopore region (pores between 2 and 50 nm). Meanwhile, AC-H6, AC-H10, and AC-H14 showed multi-modal distribution, with numerous peaks in the mesopore area. In **Figure 2**, charcoal lacked a microporous structure since all pore were larger than 2 nm. All charcoal pore configurations are found in the mesopore area due to carbonization products such as tar sealing the micropores generated during the process. Meanwhile,

mesopore which are greater than the micropore, remained unsealed as shown in **Figure 2**. It is always present in charcoal and AC, serving as a link between macropores and mesopores. AC have a small number of pore distributed in the micropores (pores less than 2 nm), with the majority located in the mesopore area. However, AC-H10 had the greatest adsorption peak of 0.007 cc/g/nm at pore diameter of 1.84 nm, suggesting optimal PSD. The distribution of AC pore in the micropore and mesopore areas had been previously reported by Ma [6], Li and Xiao [38] and Shao [39].

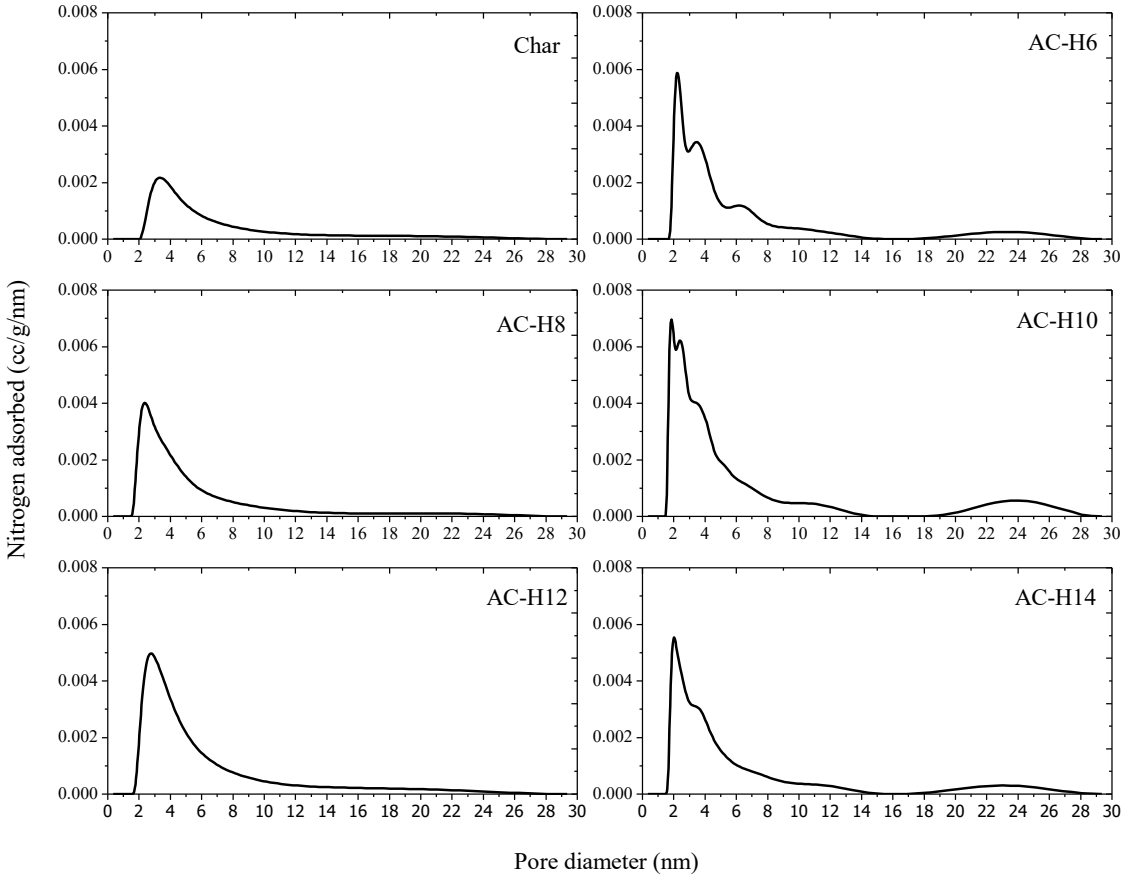

Figure 5 PSD of samples.

Surface structure of AC

Pore structure of charcoal and AC, including S_{BET}, V_P, and D_P, are shown in **Table 4**. In general, it was proven that activation heating rate produced a parabolic pattern about S_{BET} and V_P. Furthermore, AC with activation heating rate of 10 °C/min provided optimal conditions for S_{BET} and V_P. Pore surface area and volume directly influenced adsorption capacity of AC. AC-H10, with the largest pore surface area and volume of 126.279 m^2/g and 0.235 cc/g, had a nitrogen adsorption capacity of 161.25 cc/g and 0.007 cc/g/nm, respectively, as shown in **Figures 4** and **5**, including the methylene blue absorption as in **Figure 6**. However, adsorption capacity was also influenced by pore size distribution and the molecular dimensions of the adsorbed material. Effective absorption can only occur when the molecular dimensions are equal to or less than pore diameter of AC [1].

Table 4 Surface structure properties of char and AC

Samples	Surface Structure		
	S_{BET} (m^2/g)	V_P (cc/g)	D_P (nm)
Char	37.392	0.094	21.79
AC-H6	83.393	0.164	24.02
AC-H8	72.341	0.140	19.96
AC-H10	126.279	0.235	20.08
AC-H12	92.275	0.196	20.96
AC-H14	91.618	0.175	20.11

MB adsorption

Figure 6 and **Table 5** shows the average MB adsorption, and the detailed data obtained from experiments conducted 3 times, including standard deviation, calculated using Eq. (1). The effect of activation heating rate on MB adsorption is essentially the same for S_{BET}, V_P, and nitrogen adsorption, resulting in a parabolic pattern with adsorption peak at AC-H10. In addition, AC activated at 10 °C/min showed a maximum adsorption capacity of 13.46 mg/g when compared to various heating rate. This increase in adsorption of MB on AC compared to char showed the effectiveness of activation process. Furthermore, the highest MB adsorption increase of 230.71 % occurred in AC-H10. This was highly substantiated by the fact that AC-H10 showed excellent properties in terms of TGA composition, surface morphology, structure, and adsorption isotherm, including PSD.

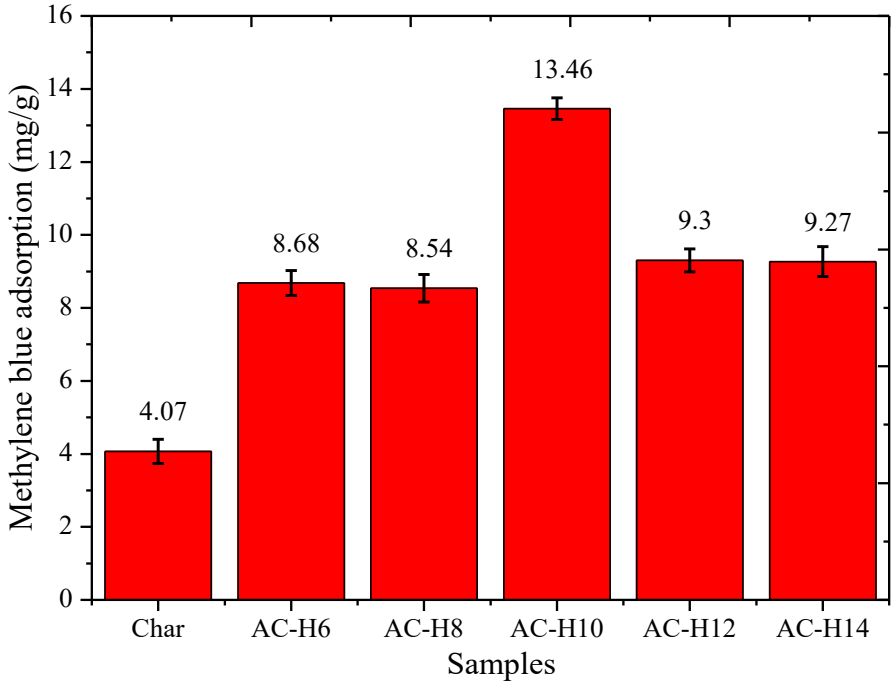

Figure 6 Methylene blue adsorption of samples.

Table 5 Adsorption of MB.

Samples	Running			Average (mg/g)	Standard Deviation
	I (mg/g)	II (mg/g)	III (mg/g)		
Char	4.38	3.61	4.22	4.07	0.33
AC-H6	8.2	8.94	8.9	8.68	0.34
AC-H8	8.58	8.98	8.06	8.54	0.38
AC-H10	13.88	13.26	13.24	13.46	0.30
AC-H12	9.48	9.56	8.86	9.3	0.31
AC-H14	9.59	8.69	9.53	9.27	0.41

Conclusions

In conclusion, this study offered a promising solution for reducing teak sawdust waste while producing AC suitable for MB adsorption. The use of various activation heating rate in the synthesis of AC had been proven to generate ideal conditions at activation rate of 10 °C/min, both in terms of properties and MB adsorption capacity. The pore were effectively cleaned of dirt at an activation rate of 10 °C/min, while the initial ones occurred without the risk of collapsing carbon framework. AC-H10 comprised 8.3 % moisture, 9 % volatile matter, 6.96 % ash, 75.74 % fixed carbon, 126.275 m^2/g specific surface area, 0.235 cc/g specific pore volume, and an average pore diameter of 20.08 nm. With the additional characteristics of multi-modal pore size distribution in the micro and meso-pore areas and an amorphous structure, AC-H10 was able to adsorb 13.46 mg/g of MB. However, further studies were needed to explore easy and cost-effective application methods and regeneration efforts before practical implementation. An important aspect of future studies should also include the analysis of kinetics, isotherms, and thermodynamics in adsorption process to develop a comprehensive understanding of real-world applications.

Acknowledgements

The authors are grateful to Udayana University's Research and Community Service Institute (LPPM) and the Faculty of Engineering at Udayana University, Indonesia for funding this study with the 2023 Study Program Leading Research (PUPS) grant under contract number B/1.469/UN14.4.A/PT.01.03.2023.

References

[1] R Mustafa and E Asmatulu. Preparation of activated carbon using fruit, paper and clothing wastes for wastewater treatment. *J. Water Process Eng*. 2020; **35**, 101239.

[2] PR Sera, PN Diagboya, SO Akpotu, FM Mtunzi, and TB Chokwe. Potential of valourized moringa oleifera seed waste modified with activated carbon for toxic metals decontamination in conventional water treatment. *Bioresour. Tech. Rep*. 2021; **16**, 100881.

[3] DNKP Negara, TGT Nindhia, M Sucipta, IW Surata, KS Astrawan and IPH Wangsa. Simultaneous adsorption of motorcycle emissions through bamboo-activated carbon. *Int. J. Glob. Energ. Issues* 2021; **43**, 199-210.

[4] Y Mochizuki, J Bud, E Byambajav and N Tsubouchi. Influence of ammonia treatment on the CO_2 adsorption of activated carbon. *J. Environ. Chem. Eng*. 2022; **10**, 107273.

[5] DNKP Negara, IM Widiyarta, IGAK Suriadi, IGK Dwijana, IMDB Penindra, IGNP Tenaya, IGK Sukadana and AS Ferdinand. Development of mesoporous activated carbons derived from brewed coffee waste for CO_2 adsorption. *Eureka Phys. Eng*. 2023; **2**, 107273.

[6] X Ma, Y Wu, M Fang, B Liu, R Chen, R Shi, Q Wu, Z Zeng and L Li. In-situ activated ultramicroporous carbon materials derived from waste biomass for CO_2 capture and benzene adsorption. *Biomass Bioenerg.* 2022; **158**, 106353.

[7] L Spessato, VA Duarte, JM Fonseca, PA Arroyo and VC Almeida. Nitrogen-doped activated carbons with high performances for CO_2 adsorption. *J. CO_2 Utilization* 2022; **61**, 102013.

[8] DNKP Negara, TGT Nindhia, IM Widiyarta, IMG Karohika, M Suarda and IGK Dwijana. Characteristics and performance analysis of activated carbons derived from different precursors and activators for waste water adsorption. *Eureka Phys. Eng*. 2023; **6**, 160-72.

[9] AA Nuhu, ICP Omali and CO Clifford. Equilibrium adsorption studies of methylene blue onto caesalpinia pulcherrima husk-based activated carbon. *Chem. Sci. Int. J*. 2019; **2**, CSIJ.39673.

[10] DNKP Negara, IM Widiyarta, IMG Karohika, IGAK Suriadi, IGK Dwijana, IP Lokantara, IM Parwata and IK Suarsana. Preparation and characterization of pelleted and powdered activated carbons derived from used brewed coffee. *Trends Sci*. 2023; **20**, 7136.

[11] P Arjunan, M Kouthaman, K Kannan, K Diwakar, V Priyanka, R Subadevi and M Sivakumar. Study on Efficient Electrode from Electronic waste renewed carbon material for sodium battery applications. *J. Environ. Chem. Eng*. 2021; **9**, 105024.

[12] H Long, H Lin, M Yan, Y Bai, X Tong, X Kong and S Li. Adsorption and diffusion characteristics of CH_4, CO_2, and N_2 in micropores and mesopores of bituminous coal: Molecular dynamics. *Fuel* 2021; **292**, 120268.

[13] E Elaiyappillai, R Srinivasan, Y Johnbosco, P Devakumar, K Murugesan, K Kesavan and PM Johnson. Lowcost activated carbon derived from Cucumis melo fruit peel for electrochemical supercapacitor application. *Appl. Surf. Sci*. 2019; **486**, 527-38.

[14] E Taer, A Apriwandi, R Taslim, A Agutino and DA Yusra. Conversion Syzygium oleana leaves biomass waste to porous activated carbon nanosheet for boosting supercapacitor performances. *J. Mater. Res. Tech*. 2020; **9**, 13332-40.

[15] MJ Mostazo-López, R Ruiz-Rosas, T Tagaya, Y Hatakeyama, S Shiraishi, E Morallón and D Cazorla-Amorós. Nitrogen doped superactivated carbons prepared at mild conditions as electrodes for supercapacitors in organic electrolyte. *J. Carbon Res.* 2020; **6**, 56.

[16] JH Hassen, AA Baqer, NK Kareem and AY Zaeen. Biochemical study on the removal of water impurities using modified activated carbon. *Res. J. Pharm. Tech*. 2020; **13**, 1790-4.

[17] JH Hassen, MS Ferhan and AH Ayfan. Fexofenadine adsorption by activated charcoal impregnated with hydrogen peroxide. *Iraqi J. Sci.* 2020; **61**, 1245-52.

[18] JH Hassen, YM Farhan and AH Ayfan. Comparative study of levocetirizine elimination by pristine and potassium permanganate modified activated charcoal. *Int. J. Pharm. Sci. Res*. 2018; **9**, 5155-60.

[19] JH Hassen, AH Ayfan and YM Farhan. Spectroscopic evaluation of activated charcoal as a poison antidote for gliclazide drug. *Asian J. Pharm. Clin. Res.* 2018; **11**, 140-3.

[20] GJ Mcdougall. The physical nature and manufacture of activated carbon. *J. S. Afr. Inst. Min. Metall*. 1991; **91**, 109-20.

[21] IM Astika, DNKP Negara, CIPK Kencanawati, TGT Nindhia and F Hidajat. Proximate and morphology properties of swat bamboo activated carbon carburized under different carbonization temperature. *IOP Conf. Ser. Mater. Sci. Eng*. 2019; **539**, 012010.

[22] DNKP Negara, TGT Nindhia, Lusiana, IM Astika and CIPK Kencanawati. Development and characterization of activated carbons derived from lignocellulosic material. *Mater. Sci. Forum* 2020; **988**, 80-6.

[23] EH Sujiono, D Zabrian, Zurnansyah, Mulyati, V Zharvan, Samnur and NA Humairah. Fabrication and characterization of coconut shell activated carbon using variation chemical activation for wastewater treatment application. *Results Chem*. 2022; **4**, 100291.

[24] M Deng, J Wang and Q Zhang. Effect of freezing pretreatment on the performance of activated carbon from coconut shell for supercapacitor application. *Mater. Lett*. 2022; **306**, 130934.

[25] S Wang, Y Lee, Y Won, H Kim, S Jeong, BW Hwang, AR Cho, J Kim, YC Park, H Nam, D Lee, H Kim and S Jo. Development of high-performance adsorbent using KOH-impregnated rice husk-based activated carbon for indoor CO_2 adsorption. *Chem. Eng. J*. 2022; **437**, 135378.

[26] A Mukherjee, JA Okolie, C Niu, and AK Dalai. Techno - Economic analysis of activated carbon production from spent coffee grounds: Comparative evaluation of different production routes. *Energ. Convers. Manag. X* 2022; **14**, 100218.

[27] R Hossain, RK Nekouei, I Mansuri and V Sahajwalla. *In-situ* O/N-heteroatom enriched activated carbon by sustainable thermal transformation of waste coffee grounds for supercapacitor material. *J. Energ. Storage* 2022; **33**, 102113.

[28] E Taer, A Apriwandi, DR Andani and R Taslim. Solid coin-like design activated carbon nanospheres derived from shallot peel precursor for boosting supercapacitor performance. *J. Mater. Res. Tech*. 2021; **15**, 1732-41.

[29] DNKP Negara, TGT Nindhia, CIPK Kencanawati, IGAK Suriadi, IM Widiyarta, IP Lokantara and IN Budiarsa. The effect of carbonisation heating rates on the properties of N-doped teak sawdust waste activated carbon. *J. Phys. Sci*. 2023; **34**, 1-20.

[30] LCDD Medeiros, AS Pimenta, RM Braga, TKDA Carnaval, PNM Neto and DMDA Melo. Effect of pyrolysis heating rate on the chemical composition of wood vinegar from Eucalyptus urograndis and Mimosa tenuiflora. *Revista Árvore* 2019; **43**, e430408.

[31] S Lee, J Kim, W Kim and J Roh. The efffect of the heating rate during carbonization on the porosity, strength, and electrical resistivity of graphite blocks using phenolic resin as a binder. *Materials* 2022; **15**, 3259.

[32] Z Liao, Y Zhu, G Sun, L Qiu and M Zhu. Micromorphology control of the lignin-based activated carbon and the study on the pyrolysis and adsorption kinetics. *Ind. Crops Prod*. 2021; **175,** 114266.

[33] AA Shagali, S Hu, Y Wang, H Li, Y Wang, S Su and J Xiang. Comparative study on one-step pyrolysis activation of walnut shells to biochar at different heating rates. *Energ. Rep*. 2021; **7**, 388-96.

[34] GK Gupta, PK Gupta and MK Mondal. Experimental process parameters optimization and in-depth product characterizations for teak sawdust pyrolysis. *Waste Manag*. 2019; **87**, 499-511.

[35] NFSM Azani, CTH Chuin, NS Abdullah, SS Sharifuddin and MH Hussin. Characterisation and kinetic studies on activated carbon derived from rubber seed shell for the removal of methylene blue in aqueous solutions. *J. Phys. Sci.* 2019; **30**, 1-20

[36] U Im, J Kim, SH Lee, S Lee, B Lee, D Peck and D Jung. Preparation of activated carbon from needle coke via two-stage steam activation process. *Mater. Lett*. 2019; **237**, 22-5.

[37] B Kaur, RK Gupta, and H Bhunia. Chemically activated nanoporous carbon adsorbents from waste plastic for CO_2 capture: Breakthrough adsorption study. *Micropor. Mesopor. Mater.* 2019; **282**, 146-58.

[38] M Li and R Xiao. Preparation of a dual pore structure activated carbon from rice husk char as an adsorbent for CO_2 capture. *Fuel Process. Tech*. 2019; **186**, 35-9.

[39] J Shao, C Ma, J Zhao, L Wang and X Hu. Effective nitrogen and sulfur co-doped porous carbonaceous CO_2 adsorbents derived from amino acid. *Colloids Surf. A Physicochem. Eng. Asp*. 2021; **632**, 127750.